Journal of Power Sources 207 (2012) 216–221

Contents lists available at SciVerse ScienceDirect

Journal of Power Sources

journal homepage: www.elsevier.com/locate/jpowsour

Ionic liquid-tethered nanoparticle/poly(ionic liquid) electrolytes for quasi-solid-state dye-sensitized solar cells

Xiaojian Chen[a,1], Qing Li[a,1], Jie Zhao[a], Lihua Qiu[a], Yueguang Zhang[a], Baoquan Sun[b], Feng Yan[a,*]

[a] Jiangsu Key Laboratory of Advanced Functional Polymer Design and Application, Department of Polymer Science and Engineering, College of Chemistry, Chemical Engineering and Materials Science, Suzhou 215123, China
[b] Jiangsu Key Laboratory of Carbon-Based Functional Materials & Devices, Institute of Functional Nano & Soft Materials (FUNSOM), Soochow University, Suzhou 215123, China

ARTICLE INFO

Article history:
Received 21 November 2011
Received in revised form
31 December 2011
Accepted 27 January 2012
Available online 3 February 2012

Keywords:
Quasi-solid-state
Dye-sensitized solar cells
Ionic liquid-tethered nanoparticle
Poly(ionic liquids)
Nanocomposite

ABSTRACT

Ionic liquid-tethered TiO_2 nanoparticles are prepared by tethering 1-methyl-3-[(triethoxysilyl)propyl]imidazolium chloride (TMICl) to TiO_2 nanoparticles. The quasi-solid-state dye-sensitized solar cells containing 15 wt% of ionic liquid-tethered nanoparticle/poly(ionic liquid) hybrid electrolytes show an overall power conversion efficiency of ~5.67% under simulated AM 1.5 solar spectrum irradiation at 50 mW cm^{-2}. Compared with unmodified TiO_2 nanoparticles, ionic liquid-tethered nanoparticle based hybrid gel electrolytes show enhanced short circuit current density (J_{sc}), open circuit voltage (V_{oc}), photoelectric conversion efficiency (η), and better long-term stability of the devices. These results indicate that the cells based on ionic liquid-tethered nanoparticle hybrid electrolytes could overcome the drawbacks of volatile liquid electrolytes, and offer a feasible method to fabricate quasi-solid-state DSSCs in future practical applications.

1. Introduction

Dye-sensitized solar cells (DSSCs) are attracting both academic and industrial interest over the past decades due to their high-efficiency and potential low-cost [1]. Overall photoelectric conversion efficiency up to 12% of DSSCs has been achieved with liquid electrolytes [2], however, there are still some scientific and technological difficulties, such as dye degradation, electrode corrosion, leakage and evaporation of organic liquid electrolytes, which restricting their practical applications [3]. To overcome these drawbacks, several methods, including p-type semiconductors [4], organic and inorganic hole conductors [5,6], gel and polymer electrolytes [7–18], have been proposed to reduce the evaporation and leakage of the liquid electrolyte by using solid or gel materials. Among these technologies, polymer based quasi-solid-state electrolytes have been attracting a great deal of interest because of their nonflammability, negligible vapor pressure, good contact with the nanocrystalline TiO_2 electrode and counter electrode [9].

More recently, growing attention has been paid to poly(ionic liquids) (poly(ILs)) because they are a new class of polymers that combine both the novel properties of ionic liquid and improved mechanical durability and dimensional control after polymerization. Poly(ILs) have been successfully applied for quasi-solid-state DSSCs which yielded high power conversion efficiency and excellent long-term stability of the devices [19,20]. Recently, it has been reported that addition of inorganic nanoparticles into the electrolytes is an effective way to improve the DSSC performance. Among the reported studies, the most commonly used are silica nanoparticles. For example, conductivity of quasi-solid-state electrolytes based on silica nanoparticle gelated ionic liquid reached the level of room temperature ionic liquid electrolyte [21]. Lin and co-workers prepared poly(ether urethane)/poly(ethylene oxide)-modified SiO_2 based electrolytes for DSSCs, and the overall power conversion efficiency of 4.86% was achieved. Compared with unmodified SiO_2 nanoparticles, the modified SiO_2 could be uniformly dispersed in polymer matrix and bring beneficial contributions to short circuit current density (J_{sc}) values and long stability of the devices [22].

Here, we report the fabrication of high-performance quasi-solid-state DSSCs using poly(ILs) which doped with ionic liquid-tethered TiO_2 nanoparticles as an electrolyte. The synthesized ionic liquid-tethered TiO_2 nanoparticle could be well dispersed in poly(ILs) to form quasi-solid-state gel electrolytes, without using any volatile organic solvents. The fabricated quasi-solid-state DSSCs show better long-term stability than that with unmodified TiO_2 nanoparticle/poly(ILs) gel electrolytes, indicating that the ionic liquid-tethered TiO_2 nanoparticle/poly(ILs) gel electrolytes are a promising candidate for solar cells with good durability.

* Corresponding author. Tel.: +86 512 65880973; fax: +86 512 65880089.
E-mail address: fyan@suda.edu.cn (F. Yan).
[1] These authors contributed equally to this work.

0378-7753/$ – see front matter © 2012 Elsevier B.V. All rights reserved.
doi:10.1016/j.jpowsour.2012.01.143

2. Experimental

2.1. Materials

Iodoethane, 1-iodopropane, 1-bromobutane, 1-methylimidazole, 1-vinylimidazole, 3-triethoxy-silylpropyl chloride, 4-tert-butylpyridine (TBP), guanidine thiocyanate (GNCS) were purchased from Alfa Aesar. Lithium bis(trifluoromethanesulfonyl) imide (LiTFSI) was kindly provided by Rhodia and used as received. TiO_2 nanoparticles (P25, Degussa, ~21 nm in diameter), 1-ethyl-3-methylimidazolium iodide (EMII), 1-propyl-3-methylimidazolium iodide (PMII), and 1-ethyl-3-methylimidazolium thiocyanate (EMISCN) were synthesized according to the previous report [23]. $TiCl_4$ and H_2PtCl_6 were purchased from Aldrich. cis-Bis(isothiocyanato) bis(2,20-bipyridyl-4,40-dicarboxylato) ruthenium(II) ($[RuL_2(NCS)_2]$) was purchased from Solaronix SA (Switzerland) and used without further purification.

2.2. Synthesis of poly(ILs)

Scheme 1 shows the synthetic procedure and chemical structures of the synthesized poly(ILs), poly(1-Butyl-3-vinylimidazolium bromide) ([PBVIm][Br]).

1-Butyl-3-vinylimidazolium bromide ([BVIm][Br]) was firstly synthesized via the reaction of 1-bromobutane with 1-vinylimidazole at room temperature for 3 days. ^{1}HNMR: (400 MHz, $CDCCl_3$): 10.98 (s, 1H), 7.77 (s, 1H), 7.50 (dd, 1H), 7.46 (m, 1H), 5.95 (m, 1H), 5.36 (m, 1H), 4.38 (t, 3H), 1.91(m, 2H), 1.37(m, 2H), 0.96 (t, 3H). Yield: 74%.

[PBVIm][Br] was prepared via free radical polymerization of 1-butyl-3-vinylimidazolium bromide in ethanol at 60 °C under a nitrogen atmosphere for 24 h [20,24]. Anion-exchange of [PBVIm][Br] with LiTFSI in aqueous solution yielded poly(1-butyl-3-vinylimidazolium bis(trifluoromethanesulfonyl) imide) ([PBVIm][TFSI]) [25–28].

2.3. Synthesis of 1-methyl-3-[(triethoxysilyl)propyl]imidazolium chloride (TMICl)

In a typical synthetic procedure (Scheme 2), a mixture of 1-methylimidazole and 3-triethoxy-silylpropyl chloride (equal molar amount) was heated at 80 °C for 24 h under nitrogen atmosphere to synthesize 1-methyl-3-[(triethoxysilyl)propyl] imidazolium chloride (TMICl) [29–31]. After cooling down, the pale-yellow viscous liquid was washed with ether and dried under vacuum for 24 h. ^{1}H NMR (400 MHz, $CDCCl_3$): δ = 9.21 (s, 1H), 7.44 (s, 1H), 7.43 (s, 1H), 4.16 (t, 2H), 3.85 (s, 3H), 3.62 (4, 6H), 1.95 (m, 2H), 1.19 (t, 9H), 0.60 (m, 2H).

2.4. Preparation of ionic liquid-tethered nanoparticles

1.2 g TMICl was added into a suspension of 2.0 g TiO_2 nanoparticles (P25) in 50 mL dry chloroform. The mixture was refluxed under nitrogen atmosphere at 80 °C for 24 h [22]. The product was centrifugated and washed with chloroform to remove the unreacted TMICl. The obtained ionic liquid-tethered TiO_2 nanoparticle is referred as IL-TiO_2 in this work.

2.5. Preparation of electrolytes

Liquid electrolyte was composed of 0.1 M I_2, 0.5 M TBP, 0.1 M GNCS, EMII/PMII/EMISCN (6:6:7, v/v/v). Then 25 wt% of [PBVIm][TFSI] was added into the liquid electrolyte and stirred at 80 °C to form a quasi-solid-state polymer gel electrolyte (electrolyte A). IL-TiO_2 or TiO_2 (P25) was added into prepared [PBVIm][TFSI] gel electrolyte, and the mixture was stirred at 80 °C for 8 h.

2.6. Fabrication of quasi-solid-state DSSCs [32,33]

The cleaned FTO glass was covered at perforated adhesive tape to control the thickness and the area of mesoporous TiO_2 film (about 0.283 cm^2). Two layers of TiO_2 particles were deposited onto cleaned FTO glass and used as photoelectrodes. A 7-μm-thick film of 20-nm-sized TiO_2 particles was deposited onto the FTO glass electrode by the doctor-blade technique. The film was dried at 125 °C for 5 min. Then, a second 5-μm-thick layer of 200-nm light-scattering anatase particles were coated on the top of the first TiO_2 layer. The resulting TiO_2 films were annealed at 500 °C for 15 min. After cooling to 80 °C, the obtained TiO_2 electrode was immersed in 0.5 mM $[RuL_2(NCS)_2]$ ethanol solution at room temperature for 24 h. Afterward, the dye-coated TiO_2 electrode was washed with anhydrous ethanol and dried with nitrogen stream. To prepare the Pt counter electrode, two drops of 2 mM H_2PtCl_6 in ethanol was placed onto the cleaned FTO glass substrate, followed by drying and annealing at 400 °C for 15 min.

DSSCs were fabricated by sandwiching gel electrolytes between a dye-sensitized TiO_2 electrode and a Pt counter electrode, which were separated by a 25 μm thick hot melt ring (Surlyn, Dupont) and sealed by heating. The gel electrolytes were heated to 80 °C under stirring until the gels completely melted. The cell internal space was filled with electrolytes via vacuum backfilling. The electrolyte

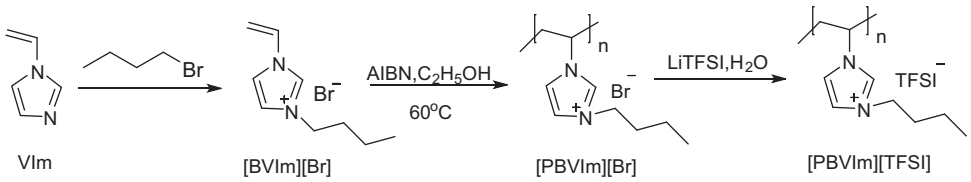

Scheme 1. General synthetic procedures for the preparation of [PBVIm][TFSI].

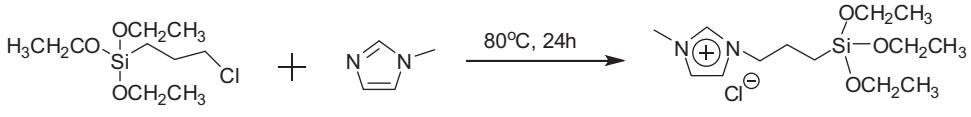

Scheme 2. General synthesis procedures for the preparation of TMICl.

injection hole on the thermally platinized FTO counter electrode was finally sealed with a Surlyn sheet and a thin glass by heating.

2.7. Characterization and photovoltaic measurements

Fourier-transform infrared (FT-IR) spectra were recorded on a ProStar LC240 FTIR spectrometer in the range of 4000–400 cm^{-1}. The conductivity of the electrolytes was characterized in an ordinary cell composed of Teflon tube and two identical stainless steel electrodes (diameter of 1 cm) on a CHI660c electrochemical workstation at room temperature, using the AC impedance method over the frequency range 1 Hz–1 MHz. The conductivity was calculated using the following equation:

$$\sigma = \frac{l}{RS} \quad (1)$$

where σ is the conductivity in S cm^{-1}, R is the ohmic resistance of the electrolyte, l is the distance between two electrodes, and S is the area of the electrodes [34].

Steady-state voltammetry was tested in a conventional photo electrochemical cell equipped with a radius of 5.0 μm platinum ultramicroelectrode (CHI107) as the working electrode, and a platinum foil as a counter electrode and reference electrode, respectively. The apparent diffusion coefficient of triiodide ($D_{app}(I_3^-)$) was calculated from the anodic and cathodic steady-state I_{ss} by using the following equation:

$$I_{ss} = 4nrFC\ D_{app} \quad (2)$$

where n is the number of electrons per molecule, F is the Faraday constant, r is the radius of the ultramicroelectrode, and C is the bulk concentration of the electroactive species [12].

The electrochemical impedance spectra (EIS) of the devices were tested using a CHI660c electrochemical workstation using the AC impedance method at the forward bias voltage for the impedance measurement was −0.70 V and the frequency ranged from 0.01–10^5 Hz under dark condition and the amplitude is 5 mV.

The photocurrent density–voltage (J–V) curves of the assembled DSSCs shielded by an aluminum foil mask with an aperture area of 0.1 cm^2 were measured with a digital source meter (Keithley, model 2612) under simulated air mass (AM) 1.5 solar spectrum illumination at 15, 50, and 100 mW cm^{-2}, respectively. Incident photo-to-current conversion efficiency (IPCE) plotted as a function of excitation wavelength was recorded on a Keithley 1612 source meter under the irradiation of a Xenon lamp with a monochromater (Oriel Cornerstone™ 260 1/4). Hermetically sealed cells were used for long-term stability tests. For thermal stress the cells were covered with UV cutoff filter, put on the magnetic heater at 60 °C and were irradiated at open circuit under one sun visible-light soaking. The photo electrochemical parameters, such as the fill factor (FF) and light-to-electricity conversion efficiency (η) were calculated according to the previous reports [35,36].

3. Results and discussion

3.1. Characterization of poly(ILs) and IL-TiO_2

Fig. 1 shows the FTIR spectra of TiO_2, TMICl and IL-TiO_2, respectively. It can be seen that a broad stretching band centered at 3434 cm^{-1} is ascribed to the hydroxyl bond (OH) groups of TiO_2 nanoparticles (Fig. 1a). An absorption peak at 1643 cm^{-1} can be assigned as TiO—H bending vibrations. The bands at 1579 and 1417 cm^{-1} are assigned to the symmetric and asymmetric stretching vibrations of carboxylate complex with surface Ti centers [37,38] (Fig. 1a). Fig. 1b shows the FTIR spectrum of TMICl. The absorption peaks at 1113 and 1168 cm^{-1} are assigned to be stretching and asymmetric stretching vibrations of C-N of imidazole rings

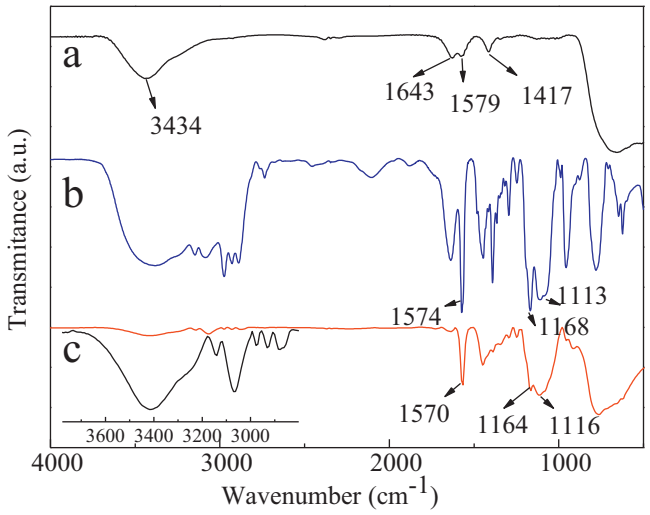

Fig. 1. FTIR spectra of (a) TiO_2 nanoparticles; (b) TMICl; (c) IL-TiO_2. The inset shows the expanded FTIR spectra of IL-TiO_2 from 2800 to 3800 cm^{-1}.

[25] (Fig. 1b). Compared with Fig. 1a and b, the hydroxyl stretching band of TiO_2 disappeared and the new bands corresponding to TMICl are observed at 1116, 1164 and 1570 cm^{-1} in Fig. 1c, indicating the successful surface modification of TiO_2 nanoparticles.

3.2. Ionic conductivity and diffusion coefficients of I_3^-

Table 1 shows the ionic conductivity and diffusion coefficients of I_3^- in [PBVIm][TFSI], IL-TiO_2/[PBVIm][TFSI] and unmodified TiO_2/[PBVIm][TFSI] based gel electrolytes at 25 °C, respectively. It can be clearly seen that both the ionic conductivity and diffusion coefficients of I_3^- increase with increasing content of IL-TiO_2, reaching a maximum ionic conductivity of 8.51×10^{-4} S cm^{-1} and diffusion coefficients of 4.55×10^{-7} cm^2 s^{-1} at 15 wt% of IL-TiO_2, respectively. It is supposed that the addition of IL-TiO_2 could form an ion transportation network in the electrolyte, which increase the movement of free ions in a regular direction and generation of free volume at the nanoparticle interface [39]. However, both two values are decreased upon the excess addition of IL-TiO_2 nanoparticles because further addition of excess inorganic fillers might aggregate and block the formed ion transport channels. Since TiO_2 fillers themselves are much less conductive than [PBVIm][TFSI], it is not surprising that excess addition of nanoparticle fillers declined the conductivity and diffusion coefficients of I_3^- [40,41]. However, compared with modified IL-TiO_2, the 15 wt% unmodified TiO_2 exhibited poor performance, because unmodified nanoparticles have huge surface energy made them prone to aggregation in the polymer matrix and made the gel unstable.

3.3. Photovoltaic performance

Fig. 2a shows the J–V curves of the DSSCs fabricated with [PBVIm][TFSI]-based gel electrolyte, IL-TiO_2/[PBVIm][TFSI] and TiO_2/[PBVIm][TFSI] gel electrolyte under simulated AM 1.5 solar spectrum illumination at 100 mW cm^{-2}, respectively. The photovoltaic parameters including open circuit voltage (V_{oc}), short circuit current density (J_{sc}), fill factor (FF), and the photoelectric conversion efficiency (η) of DSSCs are summarized in Table 1. It can be seen that the device based on [PBVIm][TFSI] electrolyte (Cell A) showed J_{sc} of 9.89 mA cm^{-2}, V_{oc} of 635 mV, FF of 0.689, and η of 4.33%. With the addition of IL-TiO_2, the J_{sc}, V_{oc} and η of the devices increased with the addition of IL-TiO_2 up to 15 wt% and decreased with the further addition. The best photovoltaic parameters were obtained for the device assembled with the electrolyte containing

Table 1
The performance of DSSCs based on different gel electrolyte under simulated AM 1.5 solar spectrum illumination at 100 mW cm^{-2}.

Cell	Electrolyte	Conductivity (10^{-4} S cm^{-1})	$D_{app}(I_3^-)$ (10^{-7} cm^2 s^{-1})	V_{oc} (mV)	J_{sc} (mA cm^{-2})	FF	η
A	0 wt% IL-TiO_2	5.6	2.99	635	9.89	0.689	4.33
B	5 wt% IL-TiO_2	6.45	3.28	637	10.48	0.706	4.72
C	10 wt% IL-TiO_2	6.83	3.63	643	10.72	0.692	4.77
D	15 wt% IL-TiO_2	8.51	4.55	659	11.66	0.683	5.26
E	20 wt% IL-TiO_2	6.79	3.76	630	11.04	0.688	4.78
F	15 wt% TiO_2	6.98	4.16	646	11.06	0.684	4.89

15 wt% IL-TiO_2 (Cell D) showed J_{sc} of 11.66 mA cm^{-2}, V_{oc} of 659 mV, FF of 0.683, and η of 5.26%. The increase in J_{sc} with the proper addition of IL-TiO_2 is related to improved diffusion coefficients of I_3^-, that the dye molecule could be regenerated more easily [42,43]. The enhanced V_{oc} is assigned from the suppression of the dark current at the TiO_2/electrolyte interface. The dark current originates from the reduction of I_3^- by conduction band electrons from TiO_2 [35]. As shown in Fig. 2b, the onset of the dark current is shifted by approx. 80 mV from cell D to cell A. The lower dark current onset value indicates the lower I_3^- reduction rate (k_{et}). The decrease of I_3^- k_{et} should lead to an increase of V_{oc} according to the following equation [20]:

$$V_{oc} = \frac{kT}{e} \ln\left(\frac{I_{inj}}{n_{cb} k_{et} [I_3^-]}\right) \quad (3)$$

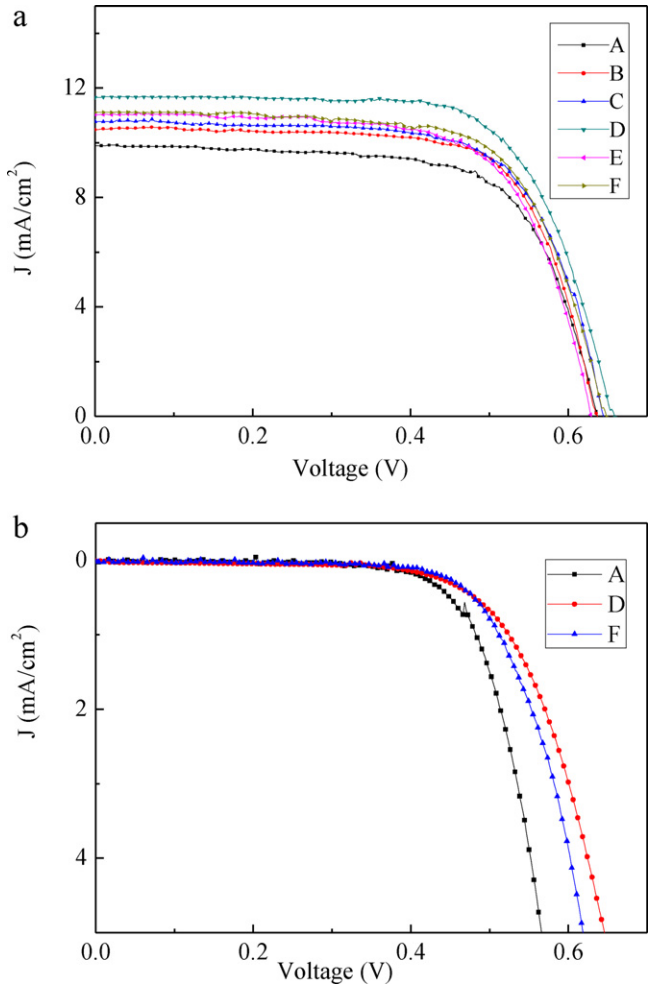

Fig. 2. The *J–V* curves of DSSCs assembled with different gel electrolyte (a) under simulated AM 1.5 solar spectrum irradiation at 100 mW cm^{-2}; (b) in the dark. Cells are tested using an aluminum foil mask with an aperture area of 0.1 cm^2.

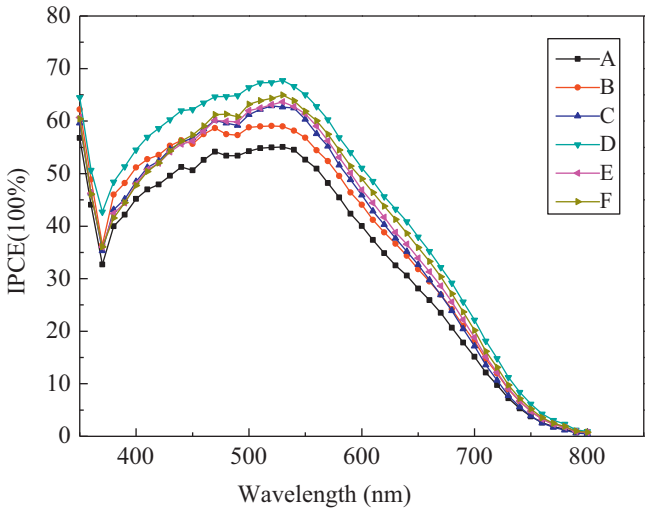

Fig. 3. The IPCE curves of DSSCs based on different gel electrolytes.

where I_{inj} is the flux of charge resulting from sensitized injection related to the electron back transfer rate, n_{cb} is the concentration of electrons at the TiO_2 surface, and k_{et} is the rate constants for I_3^- reduction. The modification of IL on TiO_2 nanoparticle surface might cause a negative shift of the TiO_2 Fermi level and suppression of the dark current at the TiO_2/electrolyte interface [44]. However, excessive addition of IL-TiO_2 decreased J_{sc} and V_{oc} because of the high viscosity and nanoparticle aggregation in the poly(ILs) electrolyte which blocked the charge transfer.

The incident photon-to-current conversion efficiency (IPCE) curves of these DSSCs are shown in Fig. 3. The maximum IPCE value as high as 67.7% at 530 nm was obtained for Cell D, which is higher than that of Cell A (55.1%), Cell B (59.1%), Cell C (62.9%), Cell E (63.6%), and Cell F (64.9%), respectively. The IPCE values of these devices are consistent with the photoelectric conversion efficiency (η). The photovoltaic performance parameters of the devices under different light intensity illumination are also summarized in Table 2. The DSSC based on electrolyte D displays a maximum η of 5.67% under the simulated air mass 1.5 solar illumination with an intensity of 50 mW cm^{-2}.

Table 2
The PCE values of DSSCs based on different electrolytes under simulated AM 1.5 solar irradiation.

Cell	1.0 sun	0.5 sun	0.15 sun
A	4.33%	4.79%	4.28%
B	4.72%	4.98%	4.40%
C	4.77%	5.06%	4.50%
D	5.26%	5.67%	4.85%
E	4.78%	5.11%	4.55%
F	4.89%	5.28%	4.68%

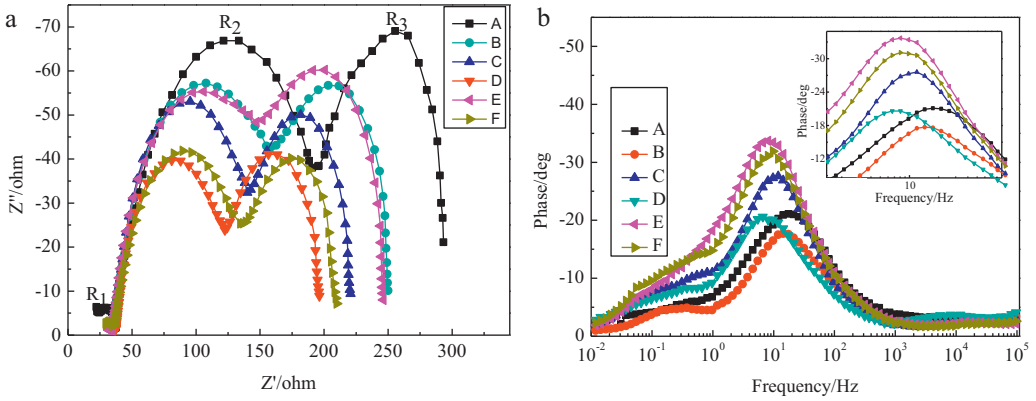

Fig. 4. The EIS Nyquist plots (a) and Bode phase plots (b) in the dark for DSSCs based on electrolytes A–F.

3.4. Electrochemical impedance spectra (EIS) of DSSCs based on different electrolytes

Electrochemical impedance spectroscopy (EIS) technique was used to reveal the appreciable difference in the charge transfer resistance at the conducting layer/TiO_2, Pt/electrolyte, dye coated TiO_2/electrolyte interface and diffusion of the I^-/I_3^- redox electrolyte, especially for understanding the recombination dynamics at the dye coated TiO_2/electrolyte [45]. Fig. 4a shows the Nyquist plot of the poly(ILs) electrolytes, IL-TiO_2/poly(ILs) and TiO_2/poly(ILs) nanocomposite gel electrolytes based cells measured at −0.7 V bias in the dark environment, and the values of resistance are listed in Table 3. From low to high frequency, three semicircles are observed in the Nyquist plots. R_1, R_2, and R_3 represent charge-transfer resistance at the counter electrode, the resistance of TiO_2/FTO, TiO_2/electrolyte interface, and the Nernst diffusion in electrolyte, respectively. It is worth noting that with the addition of IL-TiO_2 or P25 to electrolyte, the charge transport resistance at the TiO_2/electrolyte interface just decreases and reaches a minimum at 15 wt% IL-TiO_2, which is in good coordination with the reversed order observed for the photoelectric conversion efficiency (η). Among of the cells fabricated, Cell D possesses the lowest recombination resistance and enhances the charge transport at the TiO_2/electrolyte interface, as well as the enhancement of transport of I^-/I_3^- ions in the electrolyte [40].

Fig. 4b shows the Bode phase plots of EIS spectra display the characteristic frequency peaks of the charge transfer process for all cells. The effective lifetime of electrons (τ_e) before recombination in TiO_2 photoelectrode can be related to as the inverse of the characteristic frequency and estimated by the following equation [13]:

$$\tau_e = \frac{1}{\omega_{max}} = \frac{1}{2\pi f_{max}} \quad (4)$$

where f_{max} is the maximum frequency of the low-frequency peak. The maximum frequency of the middle-frequency peak (f_{max}) and lifetime of electrons are also summarized in Table 3. The electrons lifetime for recombination (τ_e) for Cell D gives the highest value of 23.96 ms, and Cell A gives the lowest value of 9.13 ms. Therefore, it can be concluded that the addition of IL-TiO_2 nanoparticles could effectively decrease electron recombination, leading to significantly enhanced electron transfer and further improved cell performance. Cell D shows the lowest recombination resistance and the longest electron lifetime, which favors the electron transport through a longer distance with less diffusive hindrance, and finally leading to enhanced photoconversion efficiency [13,46,47].

Table 3
The parameters obtained by fitting the EIS of the DSSCs fabricated with the different electrolytes.

Device	R_1 (Ω)	R_2 (Ω)	R_3 (Ω)	f_{max} (Hz)	τ_e (ms)
A	13.73	154.7	102.6	17.44	9.13
B	4.2	122.7	91.3	14.36	11.08
C	3.36	103.9	80.8	11.91	13.36
D	2.62	86.5	73.8	6.643	23.96
E	4.25	111	99.2	8.071	19.73
F	6.36	98.6	75.4	9.766	16.29

3.5. Long-term stability

The long-term stability of the quasi-solid-state DSSCs was investigated via an accelerating aging test of the sealed devices. The total efficiencies are normalized to the values measured on the first day, as shown in Fig. 5. During the first several days, the efficiency of all the cells was enhanced due to the increased regeneration rate of the dye, moderately enhanced J_{sc} and V_{oc}. It should be noted that the cell containing 15 wt% IL-TiO_2/[PBVIm][TFSI] based electrolyte (Cell D) still retains almost 100% of the initial efficiency even after about 1200 h, while the Cell A and Cell F only maintained 85% and 88% of the initial efficiency, respectively, because of the decreased J_{sc}, V_{oc} and FF values. The results revealed that the modified IL-TiO_2 nanoparticles exhibited better thermostability than the unmodified TiO_2 nanoparticles and pure poly(ILs) gel electrolyte based devices.

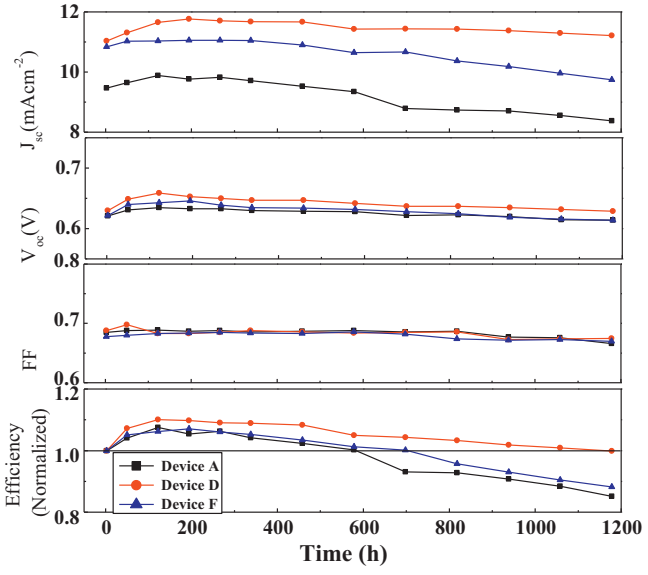

Fig. 5. Evolutions of photovoltaic performance parameters for Cells A, D and F.

4. Conclusions

In summary, poly(ILs), IL-TiO_2/poly(ILs), TiO_2(P25)/poly(ILs) nanocomposite gel electrolyte have been prepared for quasi-solid-state DSSCs. The IL-tethered TiO_2 nanoparticles introduced into poly(ILs)-based electrolyte is a successful method to enhance the circuit current density (J_{sc}) and open circuit voltage (V_{oc}), resulting in better device performance. The effective Grotthuss mechanism increases the ionic conductivity and diffusion coefficients of I_3^- and leads to increase J_{sc} and V_{oc}, and the IL absorbed on the surface of TiO_2 can also cause the enhancement of V_{oc}. Compared with unmodified TiO_2 nanoparticles, the modified TiO_2 exhibits better photoelectricity performance and long-term stability and shows maximum efficiency of 5.67% under simulated AM 1.5 solar spectrum irradiation at 50 mW cm^{-2}. These results offer us a feasible method to quasi-solid-state DSSCs in future practical applications.

Acknowledgments

This work was supported by Natural Science Foundation of China (No. 21174102), The Natural Science Foundation of Jiangsu Province (BK2011274), Research Fund for the Doctoral Program of Higher Education (20103201110003), and the Project funded by the Priority Academic Program Development of Jiangsu Higher Education Institutions.

References

[1] B. O'regan, M. Grätzel, Nature 353 (1991) 737–740.
[2] Q. Yu, Y. Wang, Z. Yi, N. Zu, J. Zhang, M. Zhang, P. Wang, ACS Nano 4 (2010) 6032–6038.
[3] A.F. Nogueira, J.R. Durrant, M.A. De Paoli, Adv. Mater. 13 (2001) 826–830.
[4] K. Tennakone, G. Senadeera, D. De Silva, I. Kottegoda, Appl. Phys. Lett. 77 (2000) 2367–2369.
[5] C.S. Karthikeyan, H. Wietasch, M. Thelakkat, Adv. Mater. 19 (2007) 1091–1095.
[6] U. Bach, D. Lupo, P. Comte, J. Moser, F. Weiss rtel, J. Salbeck, H. Spreitzer, M. Grätzel, Nature 395 (1998) 583–585.
[7] P. Wang, S.M. Zakeeruddin, J.E. Moser, M.K. Nazeeruddin, T. Sekiguchi, M. Grätzel, Nat. Mater. 2 (2003) 402–407.
[8] H. Han, W. Liu, J. Zhang, X.Z. Zhao, Adv. Funct. Mater. 15 (2005) 1940–1944.
[9] J. Nei de Freitas, A.F. Nogueira, M.-A. De Paoli, J. Mater. Chem. 19 (2009) 5279–5294.
[10] J. Wu, Z. Lan, D. Wang, S. Hao, J. Lin, Y. Huang, S. Yin, T. Sato, Electrochim. Acta 51 (2006) 4243–4249.
[11] M. Biancardo, K. West, F.C. Krebs, Sol. Energy Mater. Sol. Cells 90 (2006) 2575–2588.
[12] M. Wang, X. Pan, X. Fang, L. Guo, C. Zhang, Y. Huang, Z. Huo, S. Dai, J. Power Sources 196 (2011) 5784–5791.
[13] J. Xia, N. Masaki, M. Lira-Cantu, Y. Kim, K. Jiang, S. Yanagida, J. Am. Chem. Soc. 130 (2008) 1258–1263.
[14] C.L. Chen, H. Teng, Y.L. Lee, J. Mater. Chem. 21 (2011) 628–632.
[15] A. Hagfeldt, G. Boschloo, L. Sun, L. Kloo, H. Pettersson, Chem. Rev. 110 (2010) 6595–6663.
[16] Y. Yang, C. Zhou, S. Xu, H. Hu, B. Chen, J. Zhang, S. Wu, W. Liu, X. Zhao, J. Power Sources 185 (2008) 1492–1498.
[17] D.-W. Kim, Y.B. Jeong, S.-H. Kim, D.Y. Lee, J.S. Song, J. Power Sources 149 (2005) 112–116.
[18] T. Nguyen, X. Wang, J. Power Sources 195 (2010) 1024–1030.
[19] G. Wang, L. Wang, S. Zhuo, S. Fang, Y. Lin, Chem. Commun. 47 (2011) 2700–2702.
[20] J. Zhao, X. Shen, F. Yan, L. Qiu, S. Lee, B. Sun, J. Mater. Chem. 21 (2011) 7326–7330.
[21] P. Wang, S.M. Zakeeruddin, P. Comte, I. Exnar, M. Gr tzel, J. Am. Chem. Soc 125 (2003) 1166–1167.
[22] Y. Zhou, W. Xiang, S. Chen, S. Fang, X. Zhou, J. Zhang, Y. Lin, Chem. Commun. 18 (2009) 3895–3897.
[23] P. Bonhôte, A.P. Dias, N. Papageorgiou, K. Kalyanasundaram, M. Grätzel, Inorg. Chem. 35 (1996) 1168–1178.
[24] F. Yan, S. Yu, X. Zhang, L. Qiu, F. Chu, J. You, J. Lu, Chem. Mater. 21 (2009) 1480–1484.
[25] J. Zhao, F. Yan, Z. Chen, H. Diao, F. Chu, S. Yu, J. Lu, J. Polym. Sci. A: Polym. Chem. 47 (2009) 746–753.
[26] B. Lin, S. Cheng, L. Qiu, F. Yan, S. Shang, J. Lu, Chem. Mater. 22 (2010) 1807–1813.
[27] F. Chu, B. Lin, F. Yan, L. Qiu, J. Lu, J. Power Sources 196 (2011) 7979–7984.
[28] Y. Zhou, L. Qiu, Z. Deng, J. Texter, F. Yan, Macromolecules 44 (2011) 7948–7955.
[29] S. Sahoo, P. Kumar, F. Lefebvre, S. Halligudi, Tetrahedron Lett. 49 (2008) 4865–4868.
[30] A. Chrobok, S. Baj, W. Pudlo, A. Jarzebski, Appl. Catal. A: Gen. 366 (2009) 22–28.
[31] J. Yang, L. Qiu, B. Liu, Y. Peng, F. Yan, S. Shang, J. Polym. Sci.: Polym. Chem. 49 (2011) 4531–4538.
[32] J. Zhao, F. Yan, L. Qiu, Y. Zhang, X. Chen, B. Sun, Chem. Commun. 47 (2011) 11516–11518.
[33] S. Ito, T.N. Murakami, P. Comte, P. Liska, C. Grätzel, M.K. Nazeeruddin, M. Grätzel, Thin Solid Films 516 (2008) 4613–4619.
[34] Y. Zhang, J. Zhao, B. Sun, X. Chen, Q. Li, L. Qiu, F. Yan, Electrochim. Acta 61 (2012) 185–190.
[35] M.K. Nazeeruddin, A. Kay, I. Rodicio, R. Humphry-Baker, E. Mueller, P. Liska, N. Vlachopoulos, M. Graetzel, J. Am. Chem. Soc. 115 (1993) 6382–6390.
[36] S. Wang, S.P. Jiang, X. Wang, J. Guo, Electrochim. Acta 56 (2011) 1563–1569.
[37] P.D. Cozzoli, A. Kornowski, H. Weller, J. Am. Chem. Soc. 125 (2003) 14539–14548.
[38] C.H. Huang, Y.T. Yang, R.A. Doong, Microporous Mesoporous Mater. 142 (2011) 473–480.
[39] T.C. Merkel, B.D. Freeman, R.J. Spontak, Z. He, I. Pinnau, P. Meakin, A.J. Hill, Science 296 (2002) 519–522.
[40] S.J. Lim, Y.S. Kang, D.W. Kim, Electrochim. Acta 56 (2011) 2031–2035.
[41] Z. Huo, S. Dai, K. Wang, F. Kong, C. Zhang, X. Pan, X. Fang, Sol. Energy Mater. Sol. Cells 91 (2007) 1959–1965.
[42] Y. Zhu, Y. Shi, L. Wang, R. Gao, B. Ma, Y. Geng, Y. Qiu, Phys. Chem. Chem. Phys. 12 (2010) 15001–15006.
[43] Y. Shi, C. Zhan, L. Wang, B. Ma, R. Gao, Y. Zhu, Y. Qiu, Phys. Chem. Chem. Phys. 11 (2009) 4230–4235.
[44] C. Baik, D. Kim, M.S. Kang, S.O. Kang, J. Ko, M.K. Nazeeruddin, M. Grätzel, J. Photochem. Photobiol. A: Chem. 201 (2009) 168–174.
[45] C.P. Lee, L.Y. Lin, P.Y. Chen, R. Vittal, K.C. Ho, J. Mater. Chem. 20 (2010) 3619–3625.
[46] Q. Hou, Y. Zheng, J.-F. Chen, W. Zhou, J. Deng, X. Tao, J. Mater. Chem. 21 (2011) 3877–3883.
[47] J.K. Koh, J. Kim, B. Kim, J.H. Kim, E. Kim, Adv. Mater. 23 (2011) 1641–1646.